processes

MDPI

Article

An Improved ADRC Design Based on a Generalized Differentiator for a Nonlinear Hydraulic Turbine Regulating System

Jiwen Zhang [1], Shaojie Liu [2], Jingyan Li [3], Donghai Li [2] and Zhengwei Wang [1,*]

[1] State Key Laboratory of Hydroscience and Engineering, Department of Energy and Power Engineering, Tsinghua University, Beijing 100084, China; zhangjw21@mails.tsinghua.edu.cn
[2] State Key Laboratory of Power Systems, Department of Energy and Power Engineering, Tsinghua University, Beijing 100084, China
[3] Standardization Management Center, China Electrcity Council, Beijing 100761, China
* Correspondence: wzw@mail.tsinghua.edu.cn

Abstract: In recent years, with the advancement of renewable energy technologies, hydropower has assumed an increasingly important regulatory and balancing role in the power system. It plays an important role in grid frequency stability. This requires a faster response speed and superior disturbance immunity of the hydropower regulation system. The characteristics of active disturbance rejection control (ADRC) make it suitable for solving these kinds of nonlinearities, oscillations, and disturbances of hydro-generating units. The traditional ADRC has a complex structure and a large amount of parameter adjustments. In this paper, an improved ADRC based on a generalized differentiator is proposed, and the control loop consists of only the proportional and integrator. The parameters to be adjusted are reduced to two. The structure of the traditional ADRC is simplified. In several types of typical linear systems, the improved ADRC can harvest almost the same dynamic performance as the traditional ADRC. After applying the improved method to the simulation of a hydraulic turbine speed control system, a satisfactory response speed, superior anti-interference ability, and robustness are obtained.

Keywords: hydro-generator speed control; active disturbance rejection control; generalized differentiator; non-minimum phase system

check for updates

Academic Editor: Krzysztof Rogowski

Received: 19 November 2024
Revised: 22 December 2024
Accepted: 30 December 2024
Published: 2 January 2025

Citation: Zhang, J.; Liu, S.; Li, J.; Li, D.; Wang, Z. An Improved ADRC Design Based on a Generalized Differentiator for a Nonlinear Hydraulic Turbine Regulating System. *Processes* **2025**, *13*, 86. https://doi.org/10.3390/pr13010086

Copyright: © 2025 by the authors. Licensee MDPI, Basel, Switzerland. This article is an open access article distributed under the terms and conditions of the Creative Commons Attribution (CC BY) license (https://creativecommons.org/licenses/by/4.0/).

1. Introduction

As a clean and green energy source, hydropower plays an important role in electricity supply. In recent years, with the advancement of renewable energy generation technologies, more and more renewable energy sources (e.g., wind and solar) have been integrated into the power grid [1–3]. The integration of these new renewable energy sources has also made the structure of the grid more complex, thus increasing the need for grid frequency regulation. In addition to power generation, hydropower is responsible for a significant portion of regulation and balancing duties in many power systems. Thus, hydro regulation is critical to the frequency stability of the grid [4–8].

The traditional hydraulic turbine speed control system mostly adopts PID control, which is simple in principle and easy to realize. With the development of hydropower, the traditional PID control method faces multiple challenges, such as the instability of hydraulic and electric power oscillations, the nonlinear non-minimum phase characteristics of the system itself, the significant change in the turbine operating point during startup

and shutdown, and the system's weak resistance to load disturbances. All these problems affect the stability and efficiency of the system.

Therefore, a number of researchers have begun to actively explore and investigate a range of advanced control methods in the hope of achieving more accurate and stable control in hydroelectric governors [9–17]. Researchers have proposed predictive control strategies [9–11] with a view to more accurately predicting and compensating for system dynamic changes. An overdifferential geometrically accurate feedback linearization method [12] is also used to effectively solve the nonlinearity problem in the hydroelectric system and improve the control accuracy. To improve the frequency deadband problem, feed-forward control methods are introduced to improve the response speed and stability of the system by compensating the system inputs in advance [13]. Robust control methods [14] are also used to enhance the anti-interference capability of the system and ensure that the system can still maintain stable operation under complex and changing operating environments. The application of sliding mode control methods [15], on the other hand, helps to avoid the oscillation region, reduce the instability of the system, and further enhance the control performance. The study of these advanced control methods provides new ideas and directions for the performance optimization and upgrading of hydropower governors.

These control methods, although effective in improving the oscillation problem of hydropower units and enhancing the anti-interference capability of the system to different degrees, are also accompanied by some practical application challenges. The models of these advanced controllers are often relatively complex, involving a large number of mathematical operations and advanced algorithms, which put forward higher requirements for the design and implementation of the controllers. At the same time, the adjustment of parameters also becomes more difficult, requiring engineers and technicians to have profound professional knowledge and rich practical experience in order to accurately carry out parameter tuning and optimization. All these factors are not conducive to the wide application and promotion of the controller in practical engineering. Therefore, there is an urgent need to find a control method that is more suitable for practical engineering applications with superior performance.

In the late 1980s, Han Kyung-Ching [18] proposed an active disturbance rejection control (ADRC) that does not rely on an accurate mathematical model. Early ADRC research was dominated by nonlinear controllers with complex control algorithms. Based on the nonlinear ADRC, Professor Gao [19] linearized the nonlinear part to form linear active disturbance rejection control (LADRC), which promoted the application of ADRC in industry. Compared with other control algorithms, the LADRC system is simple, has fewer parameters to be rectified, and has stronger anti-jamming and decoupling ability. Scholars are actively exploring and applying ADRC in thermal engineering fields such as thermal power units [20], gas turbines [21], nuclear power units [22], fuel cells [23], and so on. In addition, satisfactory control results have been achieved in low-order fast systems such as servo control systems [24], motion control systems [25], robot control systems [26], and unmanned aerial vehicle control system [27]. The characteristics of ADRC make it suitable for solving the problems of nonlinearities, oscillations, and disturbances in hydroelectric generating units, which also facilitates the engineering applications.

It can be observed from the literature review that traditional PID control cannot effectively address the oscillation issues in the hydro-turbine speed control system. Currently, some advanced control algorithms have complex structures that are not conducive to engineering implementation. Therefore, this paper proposes an improved ADRC algorithm based on a generalized differentiator, which ensures the simplicity of the algorithm structure while effectively resolving the system oscillation problem.

In this paper, the expansion state observer (ESO) in LADRC is modified using generalized differentiators (GDs) [28]. This simplifies the structure of LADRC so that its structure contains only the proportional and integrator. In addition, the tuning method is optimized so that only one parameter needs to be adjusted, which is convenient for engineering applications. Applying this improved LADRC based on GD to the hydraulic turbine speed control system, comparing the PID with various tuning methods, the method in this paper has small overshoot and undershoot. In addition, it is less affected by perturbation when the difference in regulation time is not large.

2. Improved ADRC Based on GD

A typical second-order LADRC structure is shown in Figure 1. For a second-order LADRC controller, the controlled object can be viewed as a standard type of double integrator in series, as shown in Equation (1). The external perturbation d, the noise w, the higher-order characteristics y, and the unmodeled characteristics can be treated as a summed perturbation f.

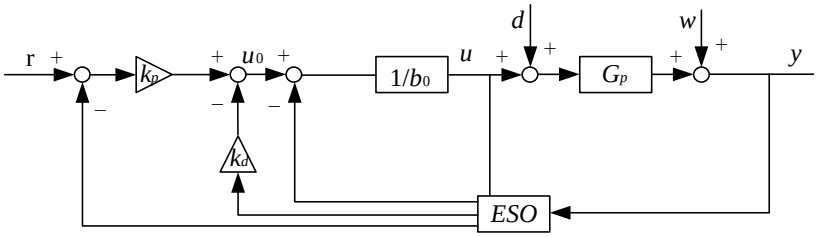


Figure 1. Typical structure of second-order LADRC.

$$\begin{cases} \dot{x}_1 = x_2 \\ \dot{x}_2 = f\left(x_1,\ x_2,\ \ldots,\ x_1^{(n)},\ d,\ w\right) + b_0 u \\ \dot{x}_3 = \dot{f} \end{cases} \tag{1}$$

For the LADRC, the third-order dilated state observer expression is as follows:

$$\begin{cases} \dot{z}_1 = z_2 + \beta_1(y - z_1) \\ \dot{z}_2 = z_3 + \beta_2(y - z_1) + b_0 u, \\ \dot{z}_3 = \beta_3(y - z_1) \end{cases} \tag{2}$$

where z_1 and z_2 are used to observe y and $\dot{y}$, respectively. z_3 is used to observe the perturbation f.

It can be seen that this third-order dilated state observer requires more parameters to be tuned. Therefore, the conventional ESO is improved by combining the idea of a generalized differentiator. The structure of the GD is shown in Figure 2. The principle of the GD can be found in Appendix A. It consists only of the proportional and integrator.

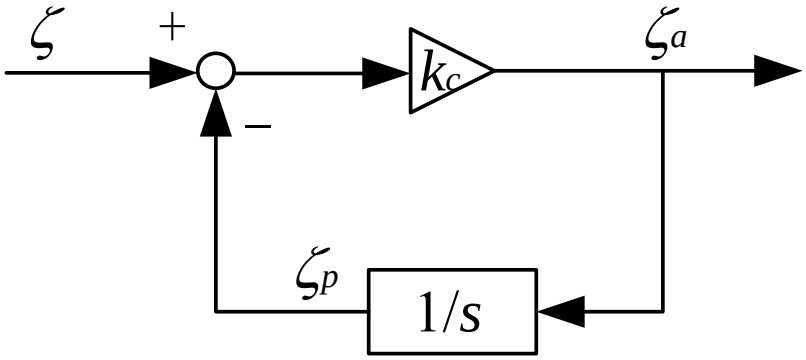


Figure 2. The structure of the generalized differentiator (GD).

ζ, ζ_a, ζ_p, and k_c are denoted as the input signal, the output signal, the feedback signal, and the gain of the GD, when $k_c \to \infty$, ζ_a approximates to the generalized derivative of ζ with respect to the time t.

The structure of the improved second-order LADRC based on GD is shown in Figure 3. z_1 and z_2 are realized by GD for observing y and $\dot{y}$, respectively. z_3 is used to observe the perturbation f.

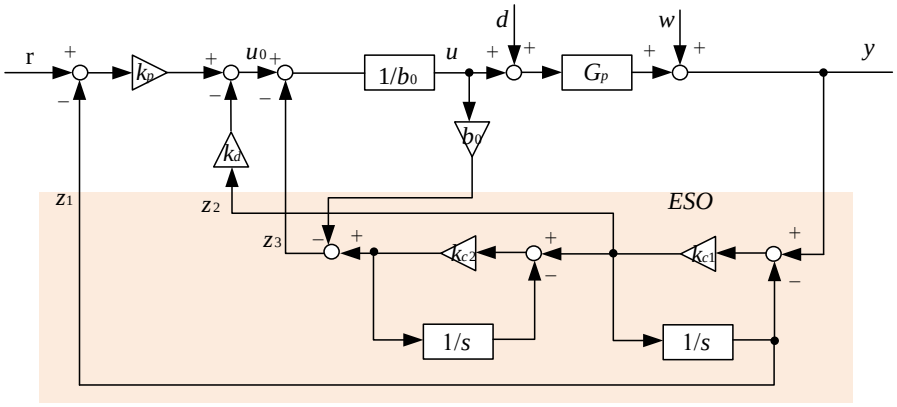


Figure 3. The structure of the improved second-order LADRC based on GD.

$$\begin{cases} \dot{z}_1 = z_2 \\ z_2 = k_c(y - z_1) \\ \dot{z}_4 = z_3 + b_0 u \\ z_3 = k_c(z_2 - z_4) - b_0 u \end{cases} \tag{3}$$

The controller part is the same as the original LADRC, so the parameterization can follow the bandwidth parameterization method of the LADRC.

$$\begin{cases} k_p = w_c^2 \\ k_d = 2 * w_c \end{cases} \tag{4}$$

The characteristic polynomial of the observer is

$$(s + k_c)(s + k_c). \tag{5}$$

Choosing the poles on $-w_o$ as the observer bandwidth, we have

$$k_c = w_o. \tag{6}$$

Most engineering objects satisfy

$$w_o \approx (2 \sim 10) w_c. \tag{7}$$

So far, the GD-based LADRC parameter tuning method is summarized as follows:

1. Based on the expected dynamics, an appropriate controller bandwidth is selected w_c.
2. The controller parameters k_p and k_d are rectified according to Equation (4).
3. We select the observer bandwidth w_o according to Equation (7).
4. The observer parameters k_c are rectified according to Equation (6).
5. We adjust b_0 so that the actual output curve of the system approaches the expected dynamic curve. If a suitable b_0 cannot be found, we reduce w_c and repeat operations 2–5.

3. Test Instance

The control effects under the improved LADRC are tested for a generalized second-order system, a non-minimum phase system, systems containing pure integral, a higher order system, and a time lag system, respectively. The transfer functions for each object are as follows:

$$G_1(s) = \frac{1}{(s+1)(0.2s+1)} \tag{8}$$

$$G_2(s) = \frac{-2s+1}{(s+0.95)^3} \tag{9}$$

$$G_3(s) = \frac{1}{s(s+1)^2} \tag{10}$$

$$G_4(s) = \frac{1}{(s+1)^7} \tag{11}$$

$$G_5(s) = e^{-10s} \frac{1}{(s+1)^2}. \tag{12}$$

The indicial response is added at t = 1 s. Then, the load step perturbation is added at 1/2 of the simulation time. The controller parameters are shown in Table 1. The dynamic response results are shown in Figure 4. The control effects are compared with the LADRC.

From the simulation result plots of many typical types of systems, it can be seen that the tracking performance curves of the LADRC improved by GD as well as the recovery curves after being subjected to transient perturbations almost coincide with the original LADRC. This shows that it is feasible to improve the LADRC using GD. The ESO function can be realized by only the proportional and integral modules. Under the premise of guaranteeing the system control effect and anti-disturbance effect, the complexity of the improved LADRC system is greatly reduced and easily realized in engineering.

Table 1. Controller parameters.

Object	Controller Parameters	
	LADRC w_c, w_o, b_0	**Improved LADRC with GD w_c, w_o, b_0**
G_1	5, 50, 2.5	5, 50, 2.5
G_2	0.78, 11.7, 10	0.78, 3.1, 10
G_3	0.5, 7.5, 0.7	0.5, 7.5, 0.7
G_4	0.5, 7.5, 3.3	0.5, 8, 3.3
G_5	0.4, 6, 4.1	0.4, 6, 4.1

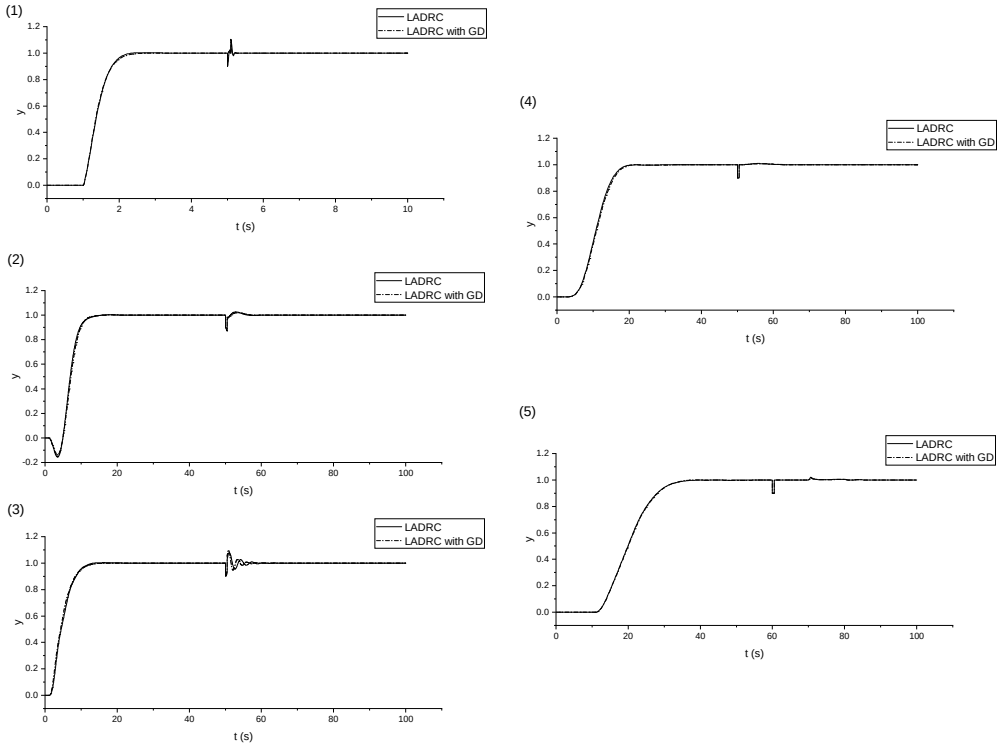


Figure 4. Response graph of the systems (Subfigure (**1**) generalized second-order system; Subfigure (**2**) nonminimum phase system; Subfigure (**3**) system with pure integral links; Subfigure (**4**) higher-order system; Subfigure (**5**) system with time-delay links.) Compared with the traditional internal mode control method, the dynamic response overshoot obtained by the improved internal mode control method is smaller, and the regulation time is shorter.

4. The Model of Turbine Regulation System

Hydropower plants are crucial facilities that transform the energy of water into electricity. They play a vital role in the power system, ensuring its safe and reliable operation. The diagram in Figure 5 illustrates the layout of a hydropower station.

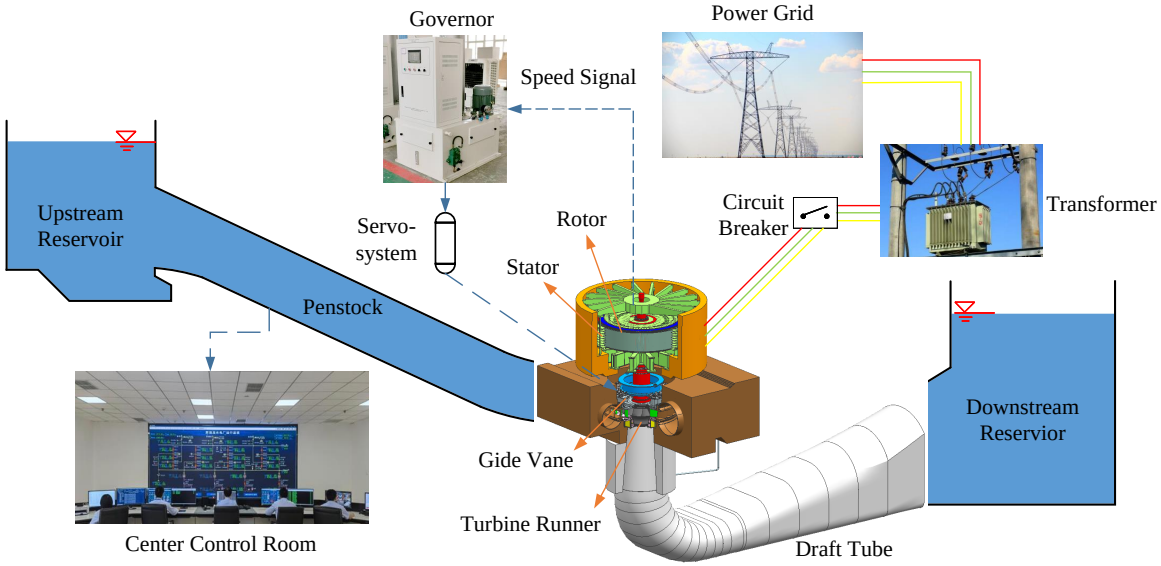


Figure 5. The block diagram of the system of hydropower plant.

In this setup, water from the reservoir upstream flows through a gate, enters the penstock system, and reaches the water inlet of the hydro turbine. The turbine blades are then turned by the water, generating mechanical energy. This energy is transferred to the synchronous generator through the main shaft, providing a continuous power source. The HTGS monitors the balance between the turbine's output and the generator's demand. If an imbalance occurs, the HTGS adjusts the guide valve's opening via relay action to maintain system stability. The HTGS focuses on studying the control mechanisms of the turbine and generator systems, and comprises the hydro-turbine, pressure water pipe, servo mechanism, controller, and synchronous generator. The block diagram of the system is shown in Figure 6, including four parts: receiver, hydraulic turbine and diversion pipeline, generator, power grid, and load.

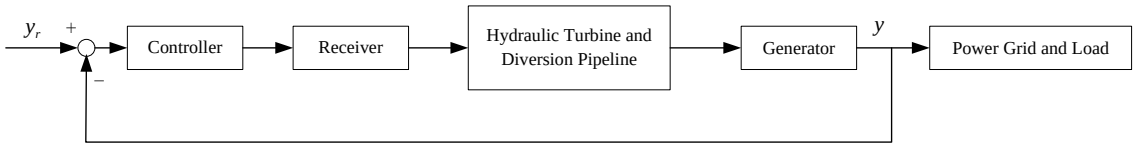


Figure 6. General layout of hydropower plant.

The receiver is the actuator of the turbine governor. Since the output of the controller is a weak control signal, it needs to be amplified by the receiver to output a displacement signal with sufficient operating force to drive the turbine water guide mechanism for regulation. The relay is usually a typical first-order inertial link with the following transfer function.

$$G_a(s) = \frac{1}{T_y s + 1}, \tag{13}$$

where T_y is the reaction time constant of the receiver. The power and flow rate of a hydraulic turbine are nonlinear functions of the guide vane opening, head, and speed. Therefore, near a given operating point, (q_0, m_0), the turbine flow (q) and torque (m) can be linearly approximated by a Taylor series as

$$\Delta m = e_y \Delta y + e_h \Delta h + e_x \Delta x \tag{14}$$

$$\Delta q = e_{qy} \Delta y + e_{qh} \Delta h + e_{qx} \Delta x, \tag{15}$$

where $e_y = \frac{\partial m}{\partial y}$ is the transfer coefficient of the turbine torque to the guide vane opening. $e_h = \frac{\partial m}{\partial h}$ is the transfer coefficient of the turbine torque to the head. $e_x = \frac{\partial m}{\partial x}$ is the transfer coefficient of turbine torque to rotational speed. $e_{qy} = \frac{\partial q}{\partial y}$ is the transfer coefficient of turbine flow to guide vane opening. $e_{qh} = \frac{\partial q}{\partial h}$ is the transfer coefficient of turbine flow to head. $e_{qx} = \frac{\partial q}{\partial x}$ is the transfer coefficient of the turbine flow to the rotational speed. The values of the turbine transfer coefficients depend on the point of the initial stabilized operating conditions, (q_0, m_0), near which they can be regarded as constants. They can be accurately obtained by field tests or by utilizing the comprehensive characteristic curve diagram of a hydraulic turbine. The characteristics of the water flow in the diversion pipeline greatly affect the performance of the turbine regulation system. The change in the turbine head H due to the change in the flow velocity V without considering the elastic water strike effect is

$$\Delta H \rho g A = -\rho A L \frac{d\Delta V}{dt}. \tag{16}$$

The initial flow rate V_0 and initial head H_0 are introduced at both ends of the above equation and rewritten in relative value form.

$$\Delta h = -\frac{LV_0}{gH_0}\frac{d\Delta v}{dt} = -T_w\frac{d\Delta q}{dt} \tag{17}$$

$$F(s) = \frac{\Delta h(s)}{\Delta q(s)} = -T_w s, \tag{18}$$

where T_w is the water flow inertia time constant. When the elastic water hammer is considered and the pressure pipe is assumed to have a uniform wall, the head and flow changes at the turbine inlet have the following relationship.

$$F(s) = \frac{\Delta h(s)}{\Delta q(s)} = -\frac{T_w}{T_e}\tanh(T_e s + f), \tag{19}$$

where T_e represents the transmission time of the pressure wave throughout the pipe. f represents the coefficient of friction of the pressure pipe. Expanding the above equation in terms of a Taylor series yields

$$F(s) = -\frac{T_w}{T_e}tanh(T_e s + f) = -\frac{T_w}{T_e}\frac{sinh(T_e s + f)}{cosh(T_e s + f)} = -\frac{T_w}{T_e}\frac{\sum_{n=0}^{\infty}\frac{(T_e s+f)^{2n+1}}{(2n+1)!}}{\sum_{n=0}^{\infty}\frac{(T_e s+f)^{2n}}{(2n)!}} \tag{20}$$

When $n = 0$, the above equation becomes a first-order rigid water strike equation, at which point it has good accuracy only when the frequency is less than 0.4 rad/s. When $n = 1$, the above equation becomes a third-order elastic water strike equation, at which time the resonant frequency is shifted by 0.5 rad/s. Therefore, Xuesong He [26] proposed a new low-order elastic water strike equation $F^*(s)$, which has a low order and a good approximation accuracy. This new low-order elastic water strike equation is also used for modeling in this study.

$$F^*(s) = -\frac{T_w}{T_e}\frac{\frac{2fT_e^2}{\pi^2}s^2 + T_e s + f}{\frac{4T_e^2}{\pi^2}s^2 + \frac{4fT_e}{\pi\sqrt{4+2f^2}}s + 1} \tag{21}$$

Combining the linear turbine model as well as the water strike equation $F(s)$, a complete turbine-pressure pipe linear model is shown in Figure 7.

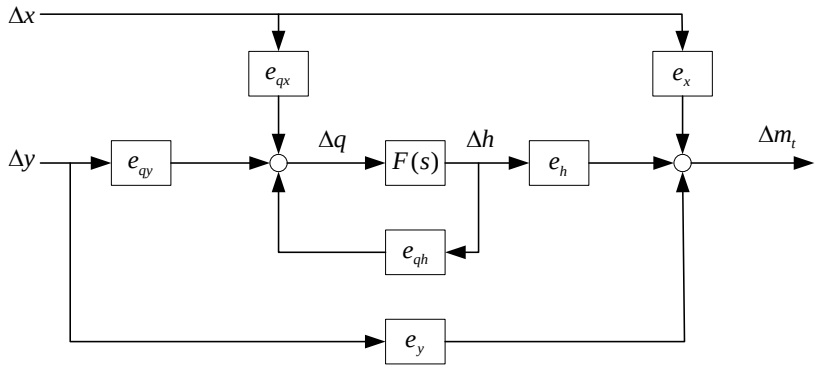


Figure 7. Turbine-pressure pipe linear model.

The hydro-generator unit operation mode is divided into a single machine isolated network operation and a grid-connected with load operation. The model transfer function of the generator load under a single machine isolated network operation is as follows.

$$G_g(s) = \frac{\Delta x_s}{\Delta p_s} = \frac{1}{T_a s + e_n}, \tag{22}$$

where T_a is the inertia time constant of the unit. e_n is the integrated self-regulation coefficient of the hydro-generator unit. When a hydroelectric generating unit is integrated into the operation of a large power grid, the unit is required to carry a specified load. In the second-order generator model, in addition to the inclusion of the mechanical inertia of the generator set, the relationship between the electromagnetic power and the power angle is also included.

$$\Delta\dot{\delta} = \omega_0 \Delta\omega \tag{23}$$

$$\Delta\dot{\omega} = \frac{1}{H}\left(\Delta P_m - D\Delta\omega - \Delta P_e\left(\delta, E^{'}\right)\right) \tag{24}$$

$$P_e\left(\delta, E^{'}\right) = \frac{E^{'} V_t}{x_d^{'}} sin\delta + \frac{V_t^2}{2}\frac{x_d^{'} - x_q}{x_d x_q}\, sin2\delta\,, \tag{25}$$

where E' is the generator transient potential. V_t is the bus voltage of the large grid. x_q is the q-axis reactance. x'_d is the d-axis transient reactance. δ is the angle at which E' exceeds V_t, i.e., the figure of merit angle. ω is the angular velocity. ω_0 is the initial angular velocity.

To summarize, the transfer function of the system when the turbine generator operates alone on the grid is

$$G(s) = \frac{1}{T_y s + 1} \cdot \frac{e_y - e_y e_{qh} F(s) + e_{qy} e_h F(s)}{1 - e_{qh} F(s)} \cdot \frac{1}{T_a s + e_n}\,. \tag{26}$$

When the turbine generator is operating in grid connection, the transfer function of the system is

$$G(s) = \frac{1}{T_y s + 1} \cdot \frac{e_y - e_y e_{qh} F(s) + e_{qy} e_h F(s)}{1 - e_{qh} F(s)} \cdot \frac{s}{T_a s^2 + \left(e_g + D_a\right)s + K_a}, \tag{27}$$

where e_g is the rate of change in the electromagnetic power with rotational speed, K_a is the equivalent synchronization coefficient, and D_a is the equivalent damping factor.

According to the above mathematical equations, the simulation model of the hydro generator set connected to the infinity grid is constructed in Simulink as shown in Figures 8 and 9.

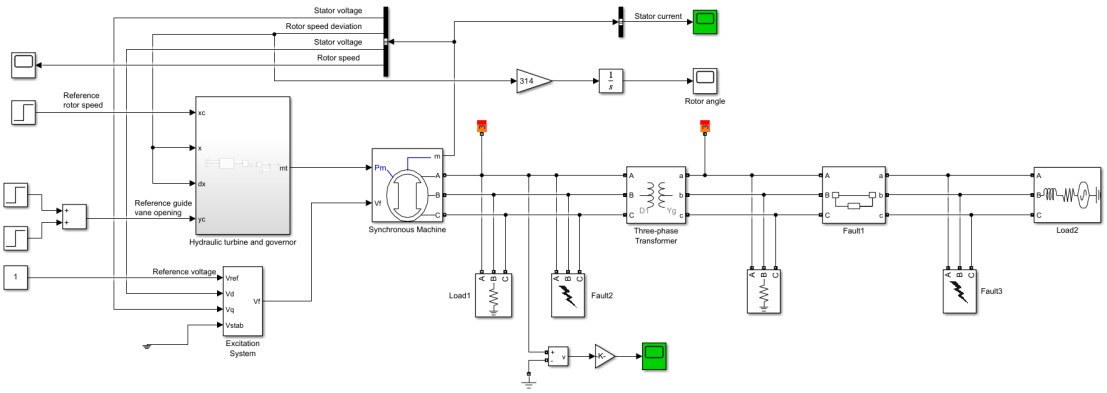


Figure 8. Simulation modeling of hydro-generator sets connected to the infinity grid.

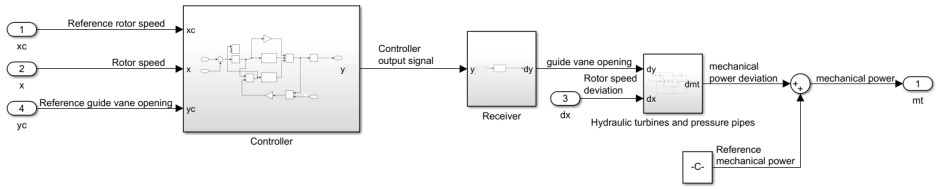


Figure 9. Simulation modeling of hydraulic turbine governor.

5. Simulation of Turbine Regulation System Based on Improved LADRC with GD

The controlled object is taken to be a certain hydro-generator unit operating in parallel with the infinity system. The specific parameters are shown in Table 2 below.

Table 2. Parameters of the system.

Mathematical Symbol	Nomenclature	Value
T_y	Reaction Time Constant of the Receiver	0.3
$e_y, e_h, e_x, e_{qy}, e_{qh}, e_{qx}$	Turbine Transfer Coefficient	1, 1.5, 0, 1, 0.5, 0
T_w	Water Flow Inertia Time Constant	1.54
T_e	Transmission Time of the Pressure Wave	0.53
T_a	Generator Inertia Time Constant	3.2
e_n	Integrated Self-regulation Coefficient	1
V_t	Bus Voltage of the Large Grid	1
E'	Generator Transient Potential	1
δ_0	Initial Angle	63.74°
ω_0	Initial Angular Velocity	314 rad/s
x'_d	d-axis Transient Reactance	1.150
x_q	q-axis Reactance	1.474

5.1. Case 1: Step Response

In this paper, the step response of HTGS is tested without connection to the grid. The step signal is added at t = 0 s. The dynamic response step results are shown in Figure 10. In addition, the control effects are compared with the conventional LADRC and PID control. The PID control was tuned by the Ziegler–Nichols (ZN) method, the gain and phase margin (GPM) specifications [29], and the particle swarm optimization algorithm, respectively. The comparative analysis of the various controllers in overshoot, undershoot, and regulation time is shown in Table 3.

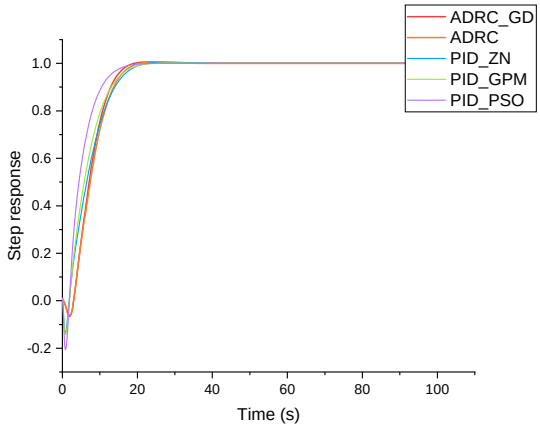


Figure 10. Dynamic response results.

Table 3. Comparative analysis of various controllers in overshoot, undershoot, and regulation time.

Controller	Overshoot (%)	Undershoot	Regulation Time (s)
LADRC with GD	0.556	−0.0657	15.02
LADRC	0.535	−0.0621	15.65
PID (ZNM)	0.527	−0.1355	16.89
PID (GPM)	0.182	−0.1432	15.65
PID (PSO)	0.030	−0.2061	12.68

The simulation results show that the improved LADRC step response curve with GD almost coincides with the LADRC curve. This indicates that it is feasible to replace the ESO method with GD for use in the turbine speed control system. In addition, from the data in the figure and table, it can be seen that compared with the other three PID governors, the LADRC improved by GD has a smaller amount of inversion and overshooting, and the regulation time is shorter, at 15.02 s. Although the PID regulation time of the parameter tuned by the particle swarm algorithm is even shorter, the undershoot is too large, which does not meet the requirements of the smoothness of hydraulic turbine governors.

Then, the performance of the LADRC and PID with different methods controllers is assessed amidst variations in the system parameters of the nonlinear HTGS. This evaluation serves to validate the robustness of the proposed LADRC with GD against fluctuations in HTGS parameters. The generator inertia time T_y of the servo-hydraulic system and the water flow inertia time T_w constant are adjusted to explore the performance of the controller. Assuming that the model parameters, T_a and T_w, undergo a 10% uptake around the nominal values, obeying a uniform distribution, 1600 Monte Carlo randomized trials are conducted, and the results of the performance distribution are shown in Figure 11. When comparing the system robustness, the main reference is the ITAE. metric of the system.

It can be seen from the figure that the ITAE of the PID with PSO is less. The PID with GPM has the second highest ITAE. Then, LADRC with GD is the third. The higher ones are the PID with ZN and LADRC. The latter four are not much different, and all of them satisfy the control requirements of the water turbine governor. The variance in the ITAE for each control method was calculated and is labeled in Figure 11. Combining the plots and the calculated data, it can be observed that the GD-based LADRC fluctuation variance is the smallest when the parameter regression occurs. The PSO-based PID with smaller ITAE has a larger fluctuation variance. The results indicate that the GD-based LADRC has superior robustness under the premise of satisfying the control requirements.

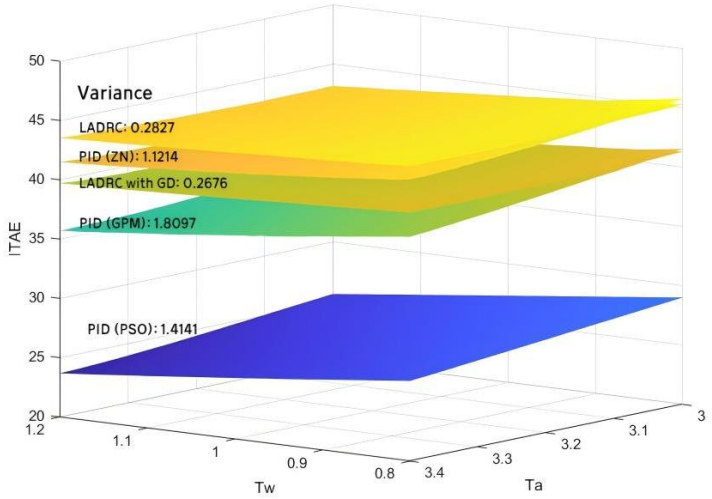


Figure 11. ITAE of HTGS with different controllers when T_a and T_w are changed.

5.2. Case 2: The Transmission Line Suddenly Tripping

In power systems, a transmission line suddenly tripping can cause disturbances to the HTGS, especially in long-distance high-capacity transmission systems. Therefore, the effect of transmission line tripping is considered in the simulation. The simulation sets the transmission line to trip at t = 0.1 s and recover at t = 0.2 s. The schematic of the line tripping fault is shown in Figure 12(1). The performance of the LADRC with GD, LADRC, and PID is shown in Figure 13. The comparative analysis of various controllers in overshoot, undershoot, and settling time under transmission line tripping is shown in Table 4. The response curve of the LADRC with GD nearly overlaps with the LADRC, which suggests that the replacement of ESO with GD is feasible. The LADRC with GD exhibits a smaller overshoot and faster response time, compared to the PID control with different tuning methods. Therefore, the LADRC with GD can effectively stabilize the HTRS with better dynamic characteristics.

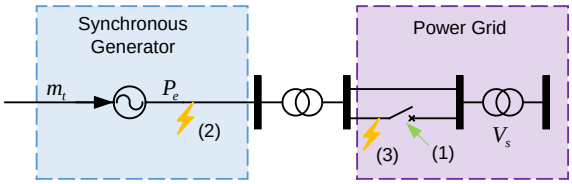


Figure 12. Simulation fault types for HTGS. Fault (1) is the transmission line suddenly tripping. Fault (2) is a three-phase short-circuit fault at the end of the synchronous generator. Fault (3) is a severe short-circuit fault in the middle of the transmission line.

Table 4. Comparative analysis of various controllers in overshoot, undershoot, and settling time under different system faults.

Scenario	Controller	Overshoot		Undershoot		Settling Time (s)	
		$\Delta\delta$	$\Delta\omega$	$\Delta\delta$	$\Delta\omega$	$\Delta\delta$	$\Delta\omega$
Fault (1)	LADRC with GD	0.1935	0.0066	−0.2706	−0.0090	4.4768	4.9601
	LADRC	0.1967	0.0068	-0.2716	−0.0092	4.4076	4.8968
	PID (ZN)	0.2221	0.0073	−0.2813	−0.0.0094	6.3668	6.8719
	PID (GPM)	0.2217	0.0073	−0.2812	−0.0094	6.3668	6.8719
	PID (PSO)	0.2208	0.0073	−0.2808	−0.0093	6.1093	6.5403
Fault (2)	LADRC with GD	0.2853	0.0088	−0.3430	−0.0103	4.7793	5.1302
	LADRC	0.2895	0.0.0091	−0.3466	−0.0104	4.7081	5.1880
	PID (ZN)	0.3104	0.0095	−0.3521	−0.0105	6.9868	7.4539
	PID (GPM)	0.3101	0.0095	−0.3521	−0.0105	6.9868	7.4539
	PID (PSO)	0.3088	0.0094	−0.3514	−0.0105	6.6901	7.1425
Fault (3)	LADRC with GD	0.3090	0.0097	−0.3808	−0.0117	5.0801	5.5801
	LADRC	0.3142	0.0100	−0.3850	−0.0119	5.0053	5.4954
	PID (ZN)	0.3388	0.0105	−0.3918	−0.0121	6.9760	7.2064
	PID (GPM)	0.3385	0.0105	−0.3918	−0.0121	6.9760	7.2064
	PID (PSO)	0.3371	0.0104	−0.3911	−0.0120	6.6798	7.0786

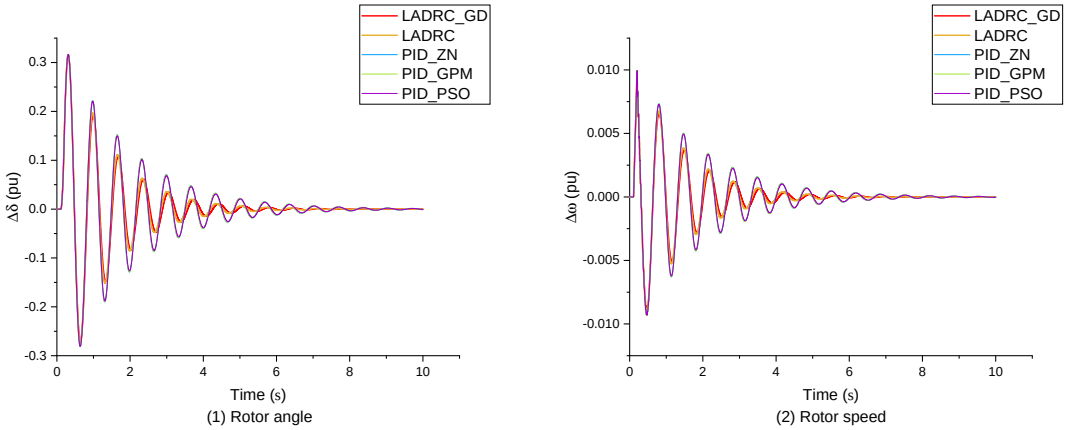


Figure 13. The performance of HTGS for the temporary tripping of a transmission line.

5.3. Case 3: Three-Phase Short-Circuit Fault at the End of the Synchronous Generator

A three-phase short circuit at the end of the generator is the most serious circuit failure. On the one hand, it causes a sudden change in current, which leads to voltage fluctuations, instability, and safety hazards on the entire grid. On the other hand, a three-phase short circuit will cause the motor excitation system to lose balance and the generator operation to be unstable. Under this fault condition, the power and output voltage of the generator are zero, which will lead to changes in the rotor angle and rotational speed of the HTGS. The simulation sets the three-phase short-circuit fault of the generator terminal at t = 0.1 s and to recover at t = 0.2 s. The schematic of three-phase short-circuit fault of the generator terminal is shown in Figure 12(2). The performance of the LADRC with GD, LADRC, and PID is shown in Figure 14. The comparative analysis of various controllers in overshoot, undershoot, and settling time under a three-phase short circuit at the end of the synchronous generator is shown in Table 4. The results indicate that employing LADRC with GD results in reduced overshoot and quicker response times in comparison to the conventional PID control methods. Consequently, the LADRC with GD proves to be highly efficient in stabilizing the HTRS with superior dynamic attributes.

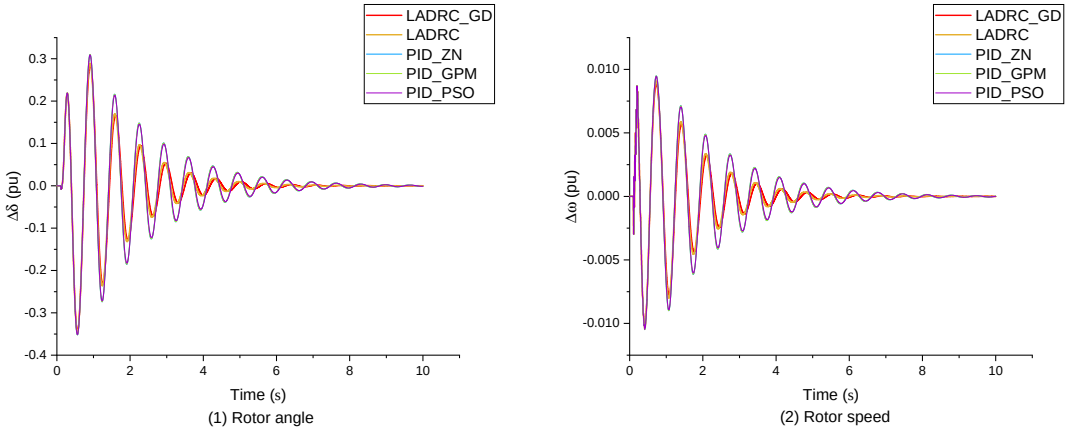


Figure 14. The performance of HTGS for the three-phase short-circuit fault on the terminal of synchronous generator.

5.4. Case 4: Severe Short-Circuit Fault in the Middle of a Transmission Line

A three-phase short circuit in the middle of a transmission line is another severe circuit failure. The voltage of the transmission line is zero, which leads to desynchronization. Therefore, the operational stability of the HTGS will be affected. The simulation sets

the short-circuit fault in the middle of transmission line at t = 0.1 s and to recover at t = 0.2 s. The schematic of the short-circuit fault in the middle of transmission line is shown in Figure 12(3). The performance of the LADRC with GD, LADRC, and PID is shown in Figure 15. The comparative analysis of various controllers in overshoot, undershoot, and settling time under a three-phase short circuit in the middle of a transmission line is shown in Table 4. The findings demonstrate that utilizing LADRC with GD diminished the overshoot and enhanced the response speed when contrasted with the traditional PID controls. Hence, LADRC with GD emerges as a potent method for stabilizing HTRS, showcasing superior dynamic qualities.

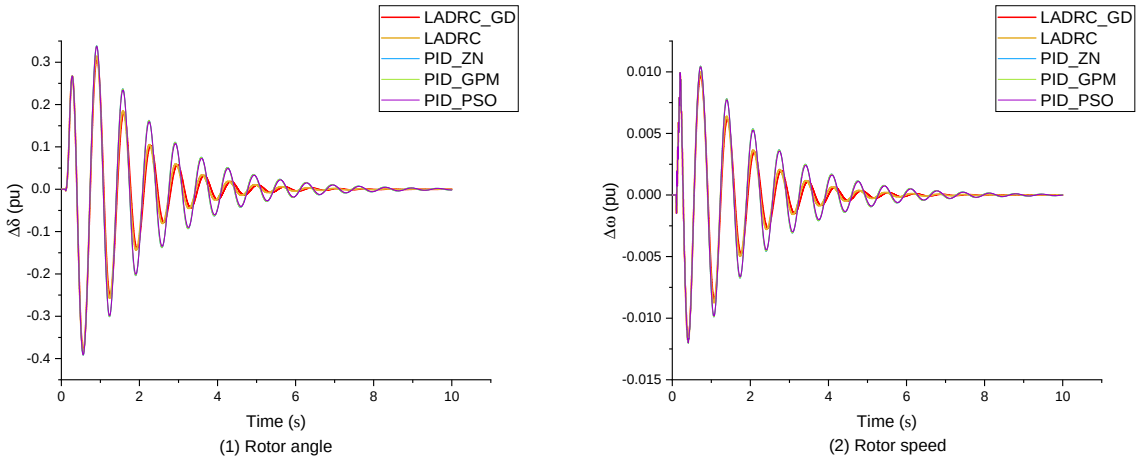


Figure 15. The performance of HTGS for the three-phase short-circuit fault in the middle of a transmission line.

Summarizing the above simulation results, it is easy to see that LADRC with GD has a similar dynamic response to LADRC, but with a simpler structure. The replacement of ESO with GD is feasible. The proposed LADRC with GD is able to perform relatively well in step response and some extreme operating conditions of HTGS. It has shorter settling time, smaller overshoot, smaller undershoot and better robustness, both in normal and extreme conditions.

6. Conclusions

In this paper, we propose a new design method for a LADRC observer. In the new method, the observer part is replaced by a GD containing only integrals and proportions. A similar function is realized with a simpler structure. Simulation tests using the new control method are performed on several types of typical systems, such as conventional second-order systems, non-minimum phase systems, systems containing pure integral terms, systems containing pure time-delay terms, and higher-order systems. The test results show that the LADRC with GD can achieve similar control effects as the original LADRC.

The method is applied to a hydraulic turbine speed control system, which is a non-minimum phase system, and is simulated in comparison with conventional PID and LADRC control. Step response tests, parameter robustness tests, and conventional grid disturbance tests are performed. The simulation results show that the LADRC with GD is similar to the conventional LADRC control. In addition, compared with the conventional PID, it has small overshoot and inversion, strong disturbance resistance, and good robustness performance.

In this study, only the HTGS problem is considered. Excitation control also exists in the water turbine power generation system. There is a coupling between the excitation system and the governor system. This coupling relationship has not been considered. Therefore, a

deeper study should be carried out in the future for the multivariable system with coupling of excitation and speed control.

Author Contributions: J.Z.: Investigation, Formal Analysis, Visualization, Writing—Original Draft, Writing—Review and Editing; S.L.: Methodology, Investigation, Formal Analysis, Validation, Writing—Review and Editing; J.L.: Investigation, Writing—Review and Editing; D.L.: Conceptualization, Supervision, Validation, Methodology, Writing—Review and Editing; Z.W.: Conceptualization, Funding Acquisition, Project Administration, Resources, Supervision. All authors have read and agreed to the published version of the manuscript.

Funding: This research received no external funding.

Data Availability Statement: Data available on request from the authors.

Conflicts of Interest: Author Jingyan Li was employed by the company Standardization Management Center, China Electrcity Council. The remaining authors declare that the research was conducted in the absence of any commercial or financial relationships that could be construed as a potential conflict of interest.

Appendix A. The Principle of GD

Definition A1. *The structure of the GD is defined as shown in Figure 2, where ζ, ζ_a, ζ_p, and k_c are denoted as the input signal, the output signal, the feedback signal, and the gain of the GD, respectively.*

Based on Definition A1, the following proposition can be proved. Then, the limit property of the GD is able to be further illustrated.

Proposition A1. *When $k_c \to \infty$, ζ_a approximates to the generalized derivative of ζ with respect to the time t.*

Proof. If $k_c \to \infty$, we have,

$$\begin{aligned} \lim_{k_c \to \infty} \zeta &= \lim_{k_c \to \infty} (\zeta_p + \frac{\zeta_a}{k_c}), \\ &= \zeta_p \end{aligned} \tag{A1}$$

which means that $\zeta \to \zeta_p$ when $k_c \to \infty$. Since ζ_a is the generalized derivative of ζ_p with respect to t, ζ_a approximates to the generalized derivative of ζ with respect to t when $k_c \to \infty$. □

References

1. Yolcan, O.O. World energy outlook and state of renewable energy: 10-Year evaluation. *Innov. Green Dev.* **2023**, *2*, 100070. [CrossRef]
2. Xie, X.; Ma, N.; Liu, W.; Zhao, W.; Xu, P.; Li, H. Functions of Energy Storage in Renewable Energy Dominated Power Systems: Review and Prospect. *J. Proc. Chin. Soc. Electr. Eng.* **2023**, *43*, 158.
3. Hassan, Q.; Viktor, P.; Al-Musawi, T.J.; Ali, B.M.; Algburi, S.; Alzoubi, H.M.; Al-Jiboory, A.K.; Sameen, A.Z.; Salman, H.M.; Jaszczur, M. The renewable energy role in the global energy Transformations. *Renew. Energy Focus* **2024**, *48*, 100545. [CrossRef]
4. Zhao, Z.; Yang, J.; Huang, Y.; Yang, W.; Ma, W.; Hou, L.; Chen, M. Improvement of regulation quality for hydro-dominated power system: Quantifying oscillation characteristic and multi-objective optimization. *Renew. Energy* **2021**, *168*, 606–631. [CrossRef]
5. Ju, J.; Nan, H.; Zhao, M.; Chen, Y. The Influence of the Ratio of Hydropower Unit Capacity on the Stability of Primary Frequency Regulation of Power Grid. In Proceedings of the 2018 IEEE 3rd Advanced Information Technology, Electronic and Automation Control Conference (IAEAC), Chongqing, China, 12–14 October 2018; pp. 1388–1392.
6. Tan, X.; Wang, H.; Xu, R.; Li, C. Frequency Stability of the Hydro-Dominated Power Grid Integrating the DFIG-based Variable-Speed Pumped Storage Unit. In Proceedings of the 2023 International Conference on Power, Communication, Computing and Networking Technologies, Wuhan, China, 24–25 September 2023; pp. 1–7.

7. Feng, C.; Mai, Z.; Wu, C.; Zheng, Y.; Zhang, N. Advantage of battery energy storage systems for assisting hydropower units to suppress the frequency fluctuations caused by wind power variations. *J. Energy Storage* **2024**, *78*, 109989. [CrossRef]
8. Beires, P.; Vasconcelos, M.; Moreira, C.; Lopes, J.P. Stability of autonomous power systems with reversible hydro power plants: A study case for large scale renewables integration. *Electr. Power Syst. Res.* **2018**, *158*, 1. [CrossRef]
9. Shi, K.; Wang, B.; Chen, H. Fuzzy generalised predictive control for a fractional-order nonlinear hydro-turbine regulating system. *IET Renew. Power Gener.* **2018**, *12*, 1708–1713. [CrossRef]
10. Tian, Y.; Wang, B.; Chen, D.; Wang, S.; Chen, P.; Yang, Y. Design of a Nonlinear Predictive Controller for a Fractional-Order Hydraulic Turbine Governing System with Mechanical Time Delay. *Energies* **2019**, *12*, 4727. [CrossRef]
11. Beus, M.; Pandžić, H. Practical Implementation of a Hydro Power Unit Active Power Regulation Based on an MPC Algorithm. *IEEE Trans. Energy Convers.* **2022**, *37*, 243–253. [CrossRef]
12. Bao, H.; Yang, J.; Fu, L.; Li, J. Study on nonlinear control of transition process of hydropower station based on differential geometry. *J. Water Resour.* **2008**, *39*, 1339–1345. [CrossRef]
13. An, H.; Yang, J.; Yang, W.; Cheng, Y.; Peng, Y. An Improved Frequency Dead Zone with Feed-Forward Control for Hydropower Units: Performance Evaluation of Primary Frequency Control. *Energies* **2019**, *12*, 1497. [CrossRef]
14. Liang, J.; Yuan, X.; Yuan, Y.; Chen, Z.; Li, Y. Nonlinear dynamic analysis and robust controller design for Francis hydraulic turbine regulating system with a straight-tube surge tank. *Mech. Syst. Signal Process.* **2017**, *85*, 927–946. [CrossRef]
15. Huang, S.; Wang, J. Robust Fixed-Time Integral Sliding Mode Control of a Nonlinear Hydraulic Turbine Regulating System. *J. Comput. Nonlinear Dyn.* **2020**, *15*, 031002. [CrossRef]
16. Liu, Z.; Yan, Z.; Zhang, H.; Xie, H.; Zou, Y.; Zheng, Y.; Xiao, Z.; Chen, F. Suppression and Analysis of Low-Frequency Oscillation in Hydropower Unit Regulation Systems with Complex Water Diversion Systems. *Energies* **2024**, *17*, 4831. [CrossRef]
17. Huang, Z.; Li, B.; Fu, W. Study on nonlinear robust control of hydropower unit regulation system using PSOGSA algorithm. *J. Hydropower Gener.* **2024**, *43*, 101–112. [CrossRef]
18. Han, J. *Self-Immunity Control Technology the Technique for Estimating and Compensating the Uncertainties*; Beijing National Defense Industry Publishing House: Beijing, China, 2008.
19. Gao, Z. Scaling and bandwidth-parameterization based controller tuning. In Proceedings of the 2003 American Control Conference, Denver, CO, USA, 4–6 June 2003; Volume 6, pp. 4989–4996.
20. Wu, Z.; Li, D.; Xue, Y.; Chen, Y. Gain scheduling design based on active disturbance rejection control for thermal power plant under full operating conditions. *Energy* **2019**, *185*, 744–762. [CrossRef]
21. Shi, G.; Wu, Z.; He, T.; Li, D.; Ding, Y.; Liu, S. Decentralized active disturbance rejection control design for the gas turbine. *Meas. Control* **2020**, *53*, 1589–1601. [CrossRef]
22. Gu, J.; Ji, N.L.; Sun, Y.J.; Tan, J.L.; Wang, D.X. A self-resilient multi-model control method for steam generator water level in nuclear power plants. *J. Power Eng.* **2012**, *32*, 373–377.
23. Zhao, D.; Zheng, Q.; Gao, F.; Bouquain, D.; Dou, M.; Miraoui, A. Disturbance decoupling control of an ultra-high speed centrifugal compressor for the air management of fuel cell systems. *Int. J. Hydrogen Energy* **2014**, *39*, 1788–1798. [CrossRef]
24. Zhang, J.; Cui, C.; Gu, S.; Wang, T.; Zhao, L. Trajectory Tracking Control of Pneumatic Servo System: A Variable Gain ADRC Approach. *IEEE Trans. Cybern.* **2023**, *53*, 6977–6986. [CrossRef] [PubMed]
25. Tian, C.; Yan, P. Sampled-data predictive ADRC design for nano motion systems with measurement time delay. *Kongzhi Lilun Yu Yingyong* **2018**, *35*, 1560.
26. Li, Y.; Chen, Z.; Liu, Z. Attitude control of a quad-rotor robot based on ADRC. *Ha'Erbin Gong Ye Da Xue Xue Bao* **2014**, *46*, 115–123.
27. Shi, Y.; Qiao, J.; Xue, L. The Stability of Coupled Four Rotor Unmanned Aerial Vehicle based on ADRC Controller. *Control Eng. China* **2019**, *26*, 2099.
28. Shi, G.; Dai, C.; Liu, S.; Li, D.; Ding, Y. The Design of a Reference Model-Based Proportional-Integral-Derivative Controller with the Generalized Derivative. In Proceedings of the 2023 23rd International Conference on Control, Automation and Systems (ICCAS), Yeosu, Republic of Korea, 17–20 October 2023; pp. 547–552. [CrossRef]
29. Ho, W.K.; Hang, C.C.; Cao, L.S. Tuning of PID controllers based on gain and phase margin specifications. *Automatica* **1995**, *31*, 497–502. [CrossRef]

Disclaimer/Publisher's Note: The statements, opinions and data contained in all publications are solely those of the individual author(s) and contributor(s) and not of MDPI and/or the editor(s). MDPI and/or the editor(s) disclaim responsibility for any injury to people or property resulting from any ideas, methods, instructions or products referred to in the content.